High-Resolution Length Fractionation of Surfactant-Dispersed Carbon Nanotubes

ARTICLE *in* ANALYTICAL CHEMISTRY · DECEMBER 2012

Impact Factor: 5.64 · DOI: 10.1021/ac303349q · Source: PubMed

analytical chemistry

Article

pubs.acs.org/ac

High-Resolution Length Fractionation of Surfactant-Dispersed Carbon Nanotubes

Constantine Y. Khripin, Xiaomin Tu, John M. Heddleston, Carlos Silvera-Batista, Angela R. Hight Walker, Jeffrey Fagan, and Ming Zheng*

National Institute of Standards and Technology, 100 Bureau Drive, Gaithersburg, Maryland 20899-8542, United States

Supporting Information

ABSTRACT: Length fractionation of colloidal single-wall carbon nanotube (SWCNT) dispersions is required for many studies. Size-exclusion chromatography (SEC) has been developed as a reliable method for high-resolution length fractionation of DNA-dispersed SWCNTs but has not been applied to surfactant-dispersed SWCNTs due to their lower dispersion stability and tendency to adsorb onto SEC stationary phases. Here, we report that SEC length fractionation can be achieved for bile salt dispersed SWCNTs by using porous silica-based beads as the stationary phase and bile salt solution as the mobile phase. We demonstrate that the SEC length sorting method can be combined with existing ultracentrifugation SWCNT sorting methods to produce "orthogonally sorted" samples, including length sorted semiconducting SWCNTs, which are important for electronics applications as well as length sorted empty-core SWCNTs. Importantly, we show that unlike simple length fractionation by SEC or any other method, orthogonal sorting produces samples of consistent quality for different length fractions, with similar UV−vis-nearIR absorption and Raman spectral features.

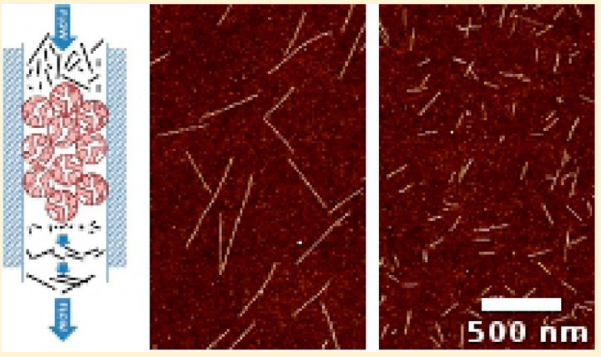

Single-wall carbon nanotubes (SWCNTs) are quasi 1-D carbon allotropes. They are typically hundreds of nanometers to micrometers long with diameters of only 1−3 nm. Many fundamental studies and applications require individualized SWCNTs, which can be obtained by colloidal dispersion of synthetic SWCNT powders using polymers or small-molecule surfactants as dispersants. These SWCNT dispersions are typically composed of tubes of broad length range, hampering many applications that require SWCNTs of a defined length range. For example, SWCNTs are being extensively explored for biomedical applications such as drug delivery, *in vitro* and *in vivo* imaging, and intracellular sensing.[1] In these applications, SWCNT length plays a significant role: long SWCNTs have been observed to have brighter fluorescence,[2] which is of interest for intracellular imaging and single-molecule detection. On the other hand, short nanotubes may be preferable for *in vivo* bioapplications where a long object could be disruptive.[3] Other phenomena that are tube length-dependent include cellular uptake of SWCNTs[4] and the recently demonstrated SWCNT self-assembly in crowded environments.[5] Furthermore, long tubes may be more useful for electronic applications,[6,7] and there are a number of recent studies on how SWCNT length influences the performance of transistors made of SWCNT networks.[8−10] Thus, it is desirable to fractionate colloidal SWCNTs by length.

Several strategies for SWCNT length fractionation have been demonstrated, including size-exclusion chromatography (SEC),[11−13] field flow fractionation,[14,15] gel chromatography,[16] ultracentrifugation,[17,18] cross-flow filtration,[19] and selective precipitation.[5] Of these methods, SEC is the only high-resolution method that can reduce tube length variation to as low as ≈10% in sorted fractions.[13] Unfortunately, this result has only been demonstrated for DNA-dispersed SWCNTs, which are very stable against flocculation.[20] In the case of the more commonly encountered surfactant-dispersed SWCNTs, high resolution length fractionation by SEC has not been shown, despite some promising early demonstrations.[12,21] This is an unfortunate limitation because commonly used surfactants for SWCNT dispersion are far less expensive than DNA, and there are well-developed methods for sorting surfactant-dispersed tubes by diameter, electronic structure, and chirality;[22−24] high resolution length fractionation is the missing link.

Early attempts using silica-based columns for SEC separation of surfactant-dispersed SWCNTs showed some promising results; however, the yield was low and many SWCNTs were found to be bundled.[11,12] In our opinion, these problems were most likely due to the use of sodium dodecyl sulfonate (SDS) as the dispersant and the mobile phase in those studies and may be eliminated by the use of a stronger surfactant such as sodium cholate (SC) or sodium deoxycholate (SDC).[25] In this report, we demonstrate that SC- and SDC-dispersed SWCNTs can indeed be effectively length-fractionated using silica-based SEC

Received: August 2, 2012
Accepted: December 22, 2012
Published: December 23, 2012

   dx.doi.org/10.1021/ac303349q | *Anal. Chem.* 2013, 85, 1382−1388

columns. We confirm the narrow length distribution of the resulting fractions with atomic force microscopy (AFM). We then demonstrate length fractionation of SWCNTs prepurified by several ultracentrifugation methods. We compare the morphology and optical qualities of these "orthogonally sorted" samples to ones obtained from unpurified SWCNTs and show that the optical absorption spectra of these mostly defect-free SWCNTs are nearly independent of SWCNT length within the range of 100−400 nm.

MATERIALS AND METHODS

Nanotube Sample Preparation. SWCNTs (grade S-P95-02-Dry, batch Du1-A001 CoMoCAT) were purchased from Southwest Nanotechnologies (Norman, OK).[26] For making surfactant-dispersed SWCNTs, a total of 40 mg of SWCNT powder were first suspended in deionized (DI) water at a concentration of 1 mg/mL by sonicating for 5 min with a 10 mm diameter probe sonicator. This stock solution was used to create 0.5 mg pellets of SWCNT material in 1 mL centrifuge tubes for dispersion. To the 0.5 mg pellet was added 1 mL of 1% SDC solution. This mixture was sonicated at 8 W with a 2 mm diameter probe for 90 min using Sonics VCX 130 (Sonics & Materials Inc., Newtown, CT). The resulting suspension was centrifuged at 18 °C and 17 000*g* in 100 μL aliquots for 120 min. The supernatant was collected and used for SEC separation.

Semiconductor-enriched arc-discharge SWCNTs (IsoNanotube-S) were purchased from NanoIntegris, Inc., Skokie, IL. The as-purchased solution was concentrated and the proprietary surfactant blend replaced with SDC by the following steps before SEC separation: 4 mL of IsoNanotube-S solution was diluted 16× with 1% SDC and concentrated to a final volume of 1 mL using a pressure cell (Amicon 8003, Millipore, Billerica, MA) with a 30 kDa cutoff filter (regenerated cellulose YM30, Millipore, Billerica, MA).

An ultracentrifugation method was used to produce a purified CoMoCAT sample from a starting material (S-P95-02 grade, batch NI6-A001, Southwest Nanotechnologies) according to a previously reported procedure.[18] This method produces samples with very high excitonic transition peaks relative to the absorption baseline and enriched in longer tubes relative to the unsorted starting materials. The purified CoMoCAT SWCNT dispersion was concentrated using a procedure similar to the one for the semiconductor-enriched sample. The resulting dispersion was used for SEC separation.

For empty/water-filled SWCNT sorting, SWCNT powder produced by the arc-discharge method was acquired from Carbon Solutions (AP grade, Riverside CA). The separation of the empty and water-filled nanotubes employed a rate-zonal separation method described previously.[27] Fractions were recovered by hand pipetting sequential layers and collecting like fractions. Pressure cells were used to remove iodixanol used for the separation and to concentrate the empty-enriched fraction through sequential dilution/concentration cycles. The resulting dispersion was used for SEC separation.

SEC Fractionation. A GE ÄKTA Purifier HPLC system in conjunction with SEC columns packed with 5 μm silica-based beads were used for fractionation. Both preparative scale (21.2 mm × 250 mm) and analytical scale (7.5 mm × 300 mm) columns were evaluated. The preparative scale columns (*SEC*-CNT) were purchased from Sepax Technologies Inc., Newark, DE. The analytical scale columns (Cosmosil CNT) were purchased from Nacalai Tesque, Inc., Kyoto, Japan. For prep scale separation, three columns with pore size of 2000 Å, 1000 Å, and 300 Å were used in series, with a flow rate of 4 mL/min, and a typical injection volume of 4 mL of SWCNT dispersion. The same column arrangement was also used to test analytical scale separation, with 0.5 mL/min flow rate and 250 μL injection. The samples were eluted with either 1% SC, 1% SDC, or 100 mmol/L NaSCN in 1% SC. The procedure was modified for the prepurified SWCNT samples to minimize sample dilution: a set of two analytical columns, 1000 Å and 300 Å, was used. Fractions of 5 mL for preparative scale and 0.5 mL for analytical scale were collected and named sequentially from A1 to A15, followed by B1 to B15.

SWCNT Characterization. UV−vis-NIR spectrometry was carried out on a Varian Cary 5000 spectrophotometer using a 10 mm path length microcuvette. For AFM characterization, silicon wafers functionalized with 3-(ethoxydimethylsilyl)-propylamine (APDMES, Sigma-Aldrich, St. Louis, MO) were used as substrates. For substrate functionalization, wafers were first cleaned in a UV−O chamber for 15 min, immersed into 1% APDMES in isopropanol for 20 min, and then rinsed with isopropanol and DI water. Finally, they were dried in an oven at 70 °C for 20 min. For SWCNT deposition, SEC fractions were diluted by 20 to 100-fold for SC-dispersed SWCNTs, 200-fold for SDC-dispersed SWCNTs, into 0.2% SC/20 mmol/L NaSCN solution. The diluted SWCNT solution was incubated on the APDMES-functionalized substrate for 6 min, and the substrate was rinsed with DI water and dried with N_2. AFM imaging was done on a Bruker Dimension Icon AFM in the peak-force tapping mode.

Nanotube curvature analysis from AFM images was performed as follows. We used the MATLAB image analysis toolkit to represent each image as a matrix of coordinates. First, each nanotube was approximated by a series of points. Next, a circle of radius R was fitted to each three point interval, and the curvature κ was calculated using the formula $\kappa = 1/R$. Finally, κ was weighted by segment length to obtain the mean curvature of the nanotube. The average curvature for each sample was calculated from the mean curvature of 100−200 SWCNTs.

For Raman spectroscopy, samples were diluted with 1% SDC to similar SWCNT concentrations as measured by UV−visible absorbance on a Perkin-Elmer Lambda 25 spectrometer. Samples were then analyzed on a Renishaw InVia Raman Spectrometer using a 632 nm He−Ne laser. All spectra were measured at 3.96 mW of power using a 20× objective (Leica) with a spot size of approximately 5 μm. Once collected, separate background signals were subtracted in the Origin 8.0 software package by using a 2-point straight line for the defect (D) and graphene peaks (G). Gaussian and Lorentzian curves were fit to the D and G peaks, respectively. The software then calculated the area and measurement error under the respective curves for each sample for comparison.

RESULTS AND DISCUSSION

SEC Separation of As-Prepared SWCNTs. SEC achieves size fractionation based on the principle of exclusion of large objects from a porous stationary phase. Briefly, an SEC column of volume V_c (Scheme 1) is packed with porous beads. When a sample containing a mixture of colloidal SWCNTs is injected into the column, the nanotubes travel through the interparticle volume V_m. Depending on their length, SWCNTs are partially excluded from the pore volume V_s. The pores are chosen such that long SWCNTs are mostly excluded from V_s and short SWCNTs are able to diffuse in and out of the pores. Thus the

dx.doi.org/10.1021/ac303349q | *Anal. Chem.* 2013, 85, 1382−1388

Scheme 1. Schematic of Size-Exclusion Chromatography of Carbon Nanotubes

effective column volume is larger for shorter SWCNTs and they elute later than long SWCNTs. The equilibrium condition, which must be satisfied for this separation to be effective, is that the time it takes for a molecule to diffuse into and out of V_s from V_m is small compared to the residence time in the column. In order for this to be true, the porous beads must be small enough so that diffusion into and out of the beads is fast compared to the run time and the SWCNT must not adsorb onto the stationary phase.

Partition of SWCNTs between the pores and the bulk liquid is characterized by the partition coefficient K, which is usually defined as the ratio of stationary phase concentration to mobile phase concentration. Equivalently, K is also the ratio of the partition function for SWCNTs within and outside the pores or the fraction of the pore volume accessible to the analyte. If the pores are modeled as an infinite network of randomly oriented plates characterized by the pore surface area to volume ratio s and the SWCNT can be approximated as a thin rod of length L, the partition coefficient K is given by[28]

$$K = \exp(-sL/4) \quad (1)$$

Ideally, s should be calculated from pore dimensions supplied by the manufacturer. In many cases only the nominal pore diameter D is given, and in this case one may assume cylindrical pore geometry to obtain the expression

$$K = \exp(-L/D) \quad (2)$$

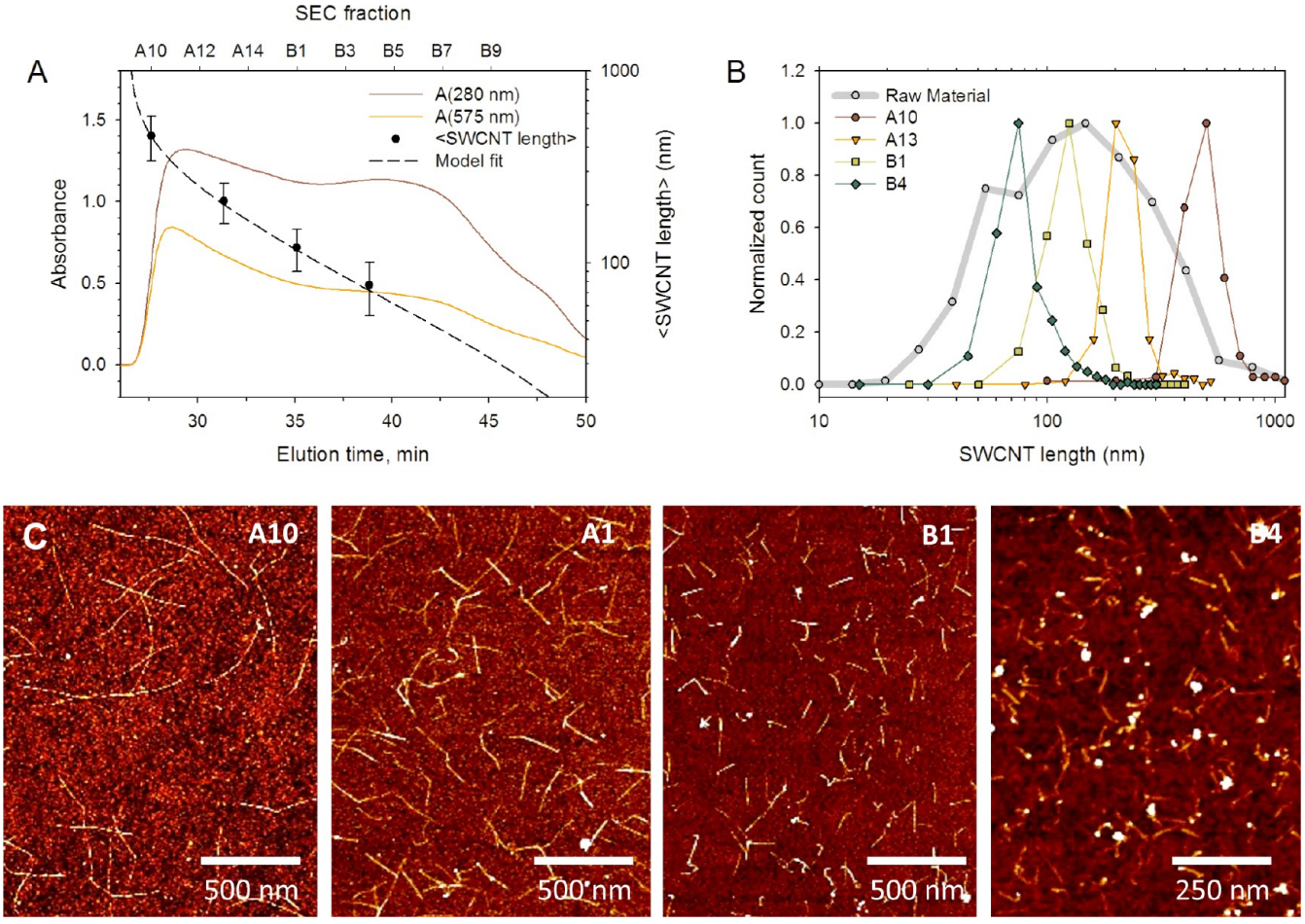

Figure 1. Length fractionation of SDC-dispersed CoMoCAT SWCNTs by SEC. (A) SEC elution profile measured by optical absorption at 280 and 575 nm. Average lengths of four representative fractions, A10, A13, B1 and B4, are also given along with predicted elution length. (B) Length distribution of the four fractions and starting material. (C) Representative AFM images.

dx.doi.org/10.1021/ac303349q | *Anal. Chem.* 2013, 85, 1382−1388

Once K is obtained for each column, the elution volume V_e for a nanotube of length L is given by

$$V_e = t_e Q = \sum_i (V_{m,i} + V_{s,i} K_i) \quad (3)$$

where t_e is the elution time and Q is the volumetric flow rate. The summation accounts for situations in which n (≥ 2) columns are arranged in series and i = 1, 2,...n. From this expression we can observe that to obtain a high resolution fractionation of nanotubes at some desired length L one must use a stationary phase with a nominal pore diameter comparable to L.

As a demonstration of this principle, we fractionated a sample of small diameter colloidal SWCNTs. A total of 2 mg of CoMoCAT SWCNTs dispersed in 4 mL of 1% SDC were injected into a series of three (D = 2000 Å, 1000 Å, 300 Å) preparative scale SEC columns. The elution profile, monitored by optical absorption at 280 and 575 nm, is shown in Figure 1A. Absorbance at 575 nm coincides with the E_{22} transition of the (6,5) chirality SWCNT, the most abundant species in the dispersion. The average SWCNT lengths of four representative fractions, derived from AFM data, are given in Figure 1A. The predicted SWCNT lengths (eq 3) are also plotted, with V_s calculated from the manufacturer's pore volume specification (1.0 cm^3/g regardless of pore size, which is also in agreement with observed V_e of small salts) and $\sum V_{m,i}$ determined from the length of the first eluting fraction. The close fit indicates that the thin, rigid rod approximation of SWCNT and the random plate approximation of the pores used in the derivation of eq 2 are both sound assumptions. Other pore geometry models, such as random network of fibers,[28] predict different behavior, with poor fractionation of long SWCNTs.

Length distribution for each of the fraction from ≈200 SWCNTs measured by AFM is plotted in Figure 1B. The length distribution of the raw material is also shown, obtained from ≈500 SWCNT measurements. Representative AFM images of the three fractions are shown in Figure 1C. Overall, the elution profile and length distributions are similar to those obtained with DNA-dispersed SWCNTs.[13] The shorter fractions contain nanotubes, but these are often curved or contain thick sections visible as white dots in the AFM image, similar to our observations in a previous report of SEC on DNA dispersed CoMoCAT.[29]

The UV−vis-NIR absorption spectra of five fractions are given in Figure 2. As with length-sorted DNA-dispersed SWCNTs, the long fractions show prominent excitonic peaks, while for shorter fractions the baseline is the dominant feature.[13,30] We have recently proposed that shorter CoMoCAT SWCNT fractions contain more defective SWCNTs, which simultaneously give rise to diminished excitonic peaks and enhanced baseline absorbance.[29] This is evident in Figure 1C, with many kinked and curved tubes in fractions B1 and B4. We have also shown in the same study that the integral of the E_{11} region (780−1350 nm) serves as the best estimate for the mass concentration of CoMoCAT SWCNTs. This method could also be used to calculate the total concentration of SWCNTs in each fraction here, if needed.

Large-scale separation using the preparative-scale columns gave similar length distributions when compared to small-scale separation using the analytical-scale columns. Both SC- and SDC-dispersed CoMoCAT SWCNTs were tested for separation, yielding similar elution profiles and quality of length sorting. For the mobile phase, we tested 1% SC, 1% SDC, and

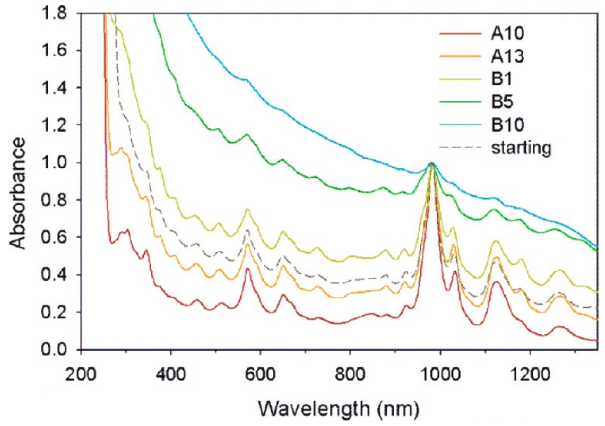

Figure 2. UV−vis-NIR spectra of SEC fractions showing prominent transition peaks for long fractions and elevated baselines for short fractions. Absorbance is scaled to 1 at the 990 nm peak feature.

1% SC plus 100 mmol/L NaSCN, which is a salt known to aid the elution of SWCNTs in ion-exchange separation.[31] We did not observe any difference among the three mobile phase compositions, and all of them yield >90% SWCNT recovery. The amount of raw material that can be purified by this method is several milligrams per run at the preparative scale; the major limiting factor is the size of available SEC columns.

Column fouling occasionally took place with the standard 5 μm bead columns, resulting in an increase in pressure drop across the column and a decrease in resolution. Inspection of disassembled columns showed that fouling occurred in the first few millimeters of the column length, suggesting that retention of very long nanotubes or nanotube aggregates was to blame. Larger beads may help alleviate this problem, but they may also reduce length resolution by increasing the time needed for equilibration between the mobile and stationary phase.[32] We tested columns with 20 μm beads and found length resolution to be similar to the 5 μm bead columns. To check the effect of equilibration time, we tested flow rates of 5 mL/min and 1.25 mL/min and observed no difference in nanotube length resolution. We also compared column loading of 5 mL (10 mg raw material) and 0.2 mL and found that resolution did not change with loading in this range. Thus 20 μm bead columns appear to be a reasonable alternative if column fouling or high pressure drop pose a problem.

SEC of Purified SWCNTs. Many purification methods have been reported for bile salt dispersed SWCNTs, such as water filled/empty fractionation,[27] low-resolution length fractionation,[17,18] and metal/semiconductor fractionation.[22] Therefore one utility of the SEC method we report here is that it can be combined with other purification methods to achieve orthogonal sorting of surfactant-dispersed SWCNTs. To illustrate this, we have conducted SEC separation of three different SWCNT dispersions prepurified by ultracentrifugation: (1) CoMoCAT SWCNTs purified and enriched in longer tubes by ultracentrifugation;[18] (2) semiconductor-enriched arc-discharge SWCNTs purified by density gradient ultracentrifugation (IsoNanotube-S, from NanoIntegris, Inc.);[33] (3) empty-enriched arc-discharge SWCNTs prepared by rate-zonal ultracentrifugation method with a step density change.[27] For these samples we used a series of two smaller columns in place of the three prep scale columns used above. The elution profiles are given in Figure S1 in the Supporting Information. As

dx.doi.org/10.1021/ac303349q | Anal. Chem. 2013, 85, 1382−1388

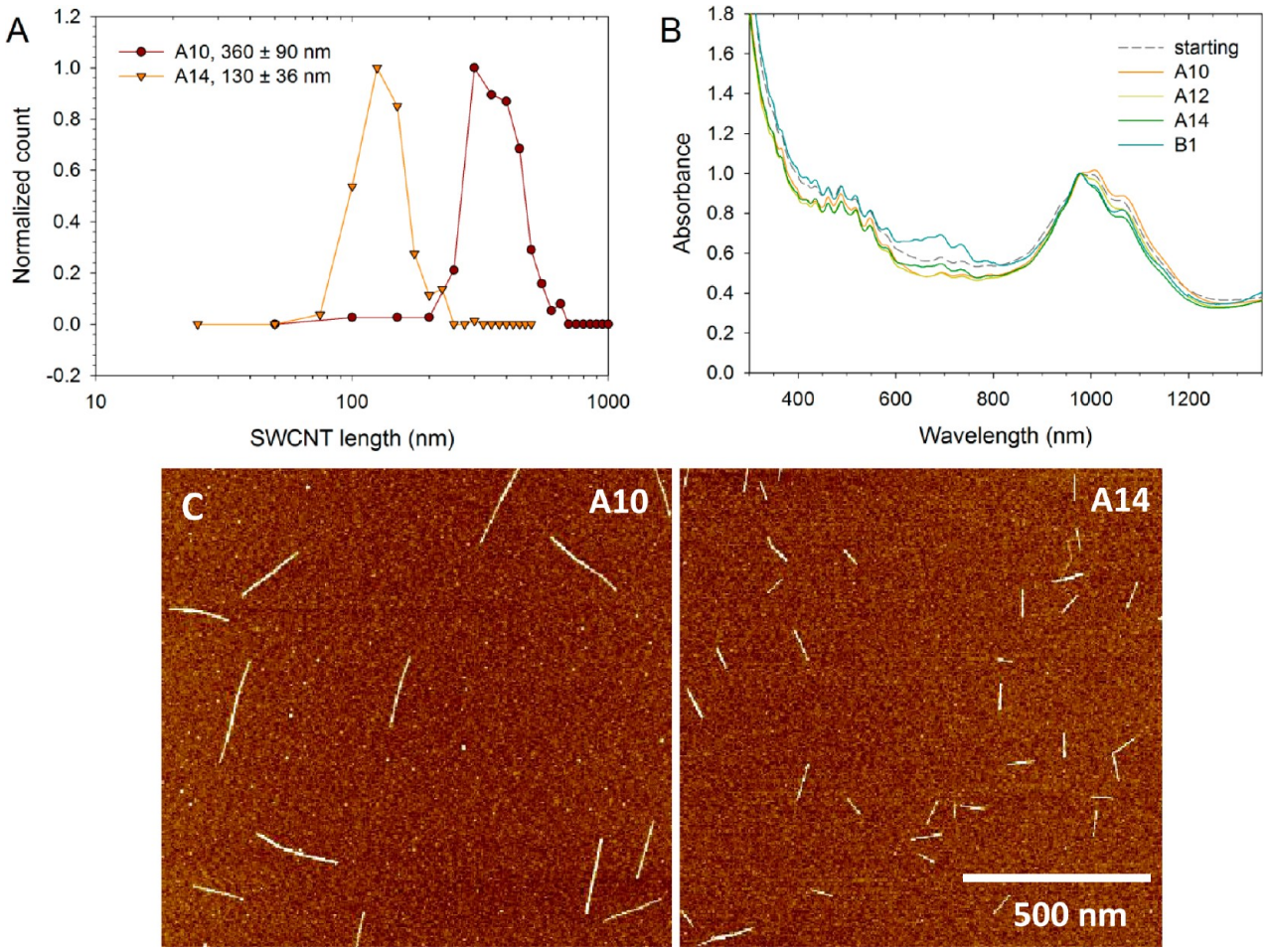

Figure 3. Length fractionation of semiconductor-enriched arc-discharge (IsoNanotube-S) SWCNTs. (A) Length distribution of two fractions A10 and A14. (B) Absorption spectra, normalized at the E_{22} transition, showing little length dependence. (C) Representative AFM images of the two fractions showing straight tubes with few contaminants.

expected, the ultracentrifugation length-fractionated sample had the narrowest elution profile.

Let us first consider the commercially available IsoNanotube-S sample. To minimize band broadening and improve sample stability, 4 mL of IsoNanotube-S solution was diluted 16× with 1% SDC and concentrated (see Materials and Methods) to a final volume of 1 mL to replace the proprietary surfactant blend with stable SDC. Length histograms of two representative fractions, absorption spectra, and AFM images are given in Figure 3. The nanotubes shown in Figure 3C appear straighter and cleaner than those in the CoMoCAT samples shown in Figure 1C. The UV−vis-NIR absorption spectra (Figure 3B) of the SEC fractions show behavior very different from the unpurified CoMoCAT samples: the baseline is essentially unchanged from long to short fractions, although some chirality redistribution is observed.

To examine the length-dependent spectral change more closely, we selected two SEC fractions from each of the four starting materials, of 360 and 130 nm average length. Figure 4 compares the absorption spectra, normalized at the highest E_{22} peak. To be quantitative, we pick the absorbance at the valley between the E_{11} and E_{22} regions (772 nm for CoMoCAT and 1280 nm for arc) as the baseline level. In the case of CoMoCAT SWCNTs (Figure 4A), the baseline of the 130 nm fraction shows a 62% increase from that of the 360 nm fraction. Similarly prepared arc nanotubes also showed a baseline increase of 23% (data not shown). We also tested a sample of HiPco SWCNTs (batch no. 195.3), and these exhibited a baseline increase of 27%.

In contrast, for the prepurified CoMoCAT (Figure 4B), the increase is only 6%, an order of magnitude lower than the change observed for the corresponding unpurified SWCNTs. In the case of semiconductor-enriched arc-discharge SWCNTs, the baseline level actually shows a 6% decrease (Figure 4C). Minor changes in chirality distribution may be the cause of the baseline decrease. For the empty-enriched arc discharge SWCNTs (Figure 4D), the baseline increase is 6%. On the basis of these observations, we conclude that in the length range of 100−400 nm, the absorption spectrum of doubly purified SWCNTs is nearly independent of length, and the upper limit of change is no higher than 6% in terms of baseline level as defined here. Thus by employing the orthogonal purification scheme, it is possible to eliminate the short-SWCNT baseline increase commonly observed in length fractionated nanotube samples.

The length-independence of SWCNT optical absorption has been proposed on several occasions.[2,13,34] However, in previous experimental studies, length fractionation invariably produced higher baselines for shorter SWCNTs.[30] To our knowledge, this is the first time length fractionated samples with consistent optical properties have been reported. What is the origin of the optical absorption baseline? Why ultracentrifugation reduces

dx.doi.org/10.1021/ac303349q | Anal. Chem. 2013, 85, 1382−1388

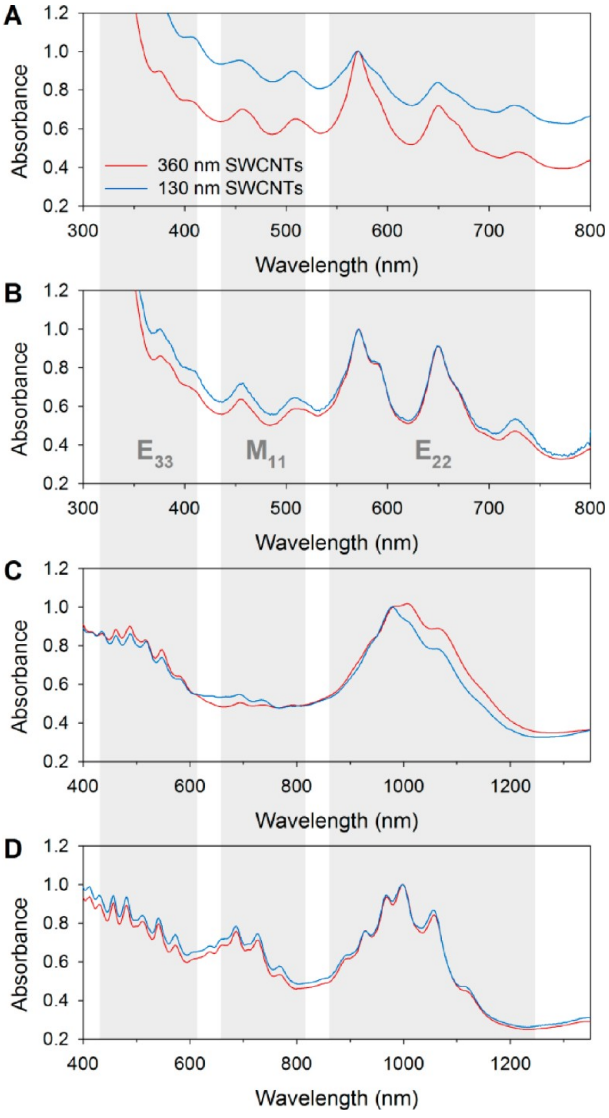

Figure 4. Optical absorption spectra of long (360 nm, red traces) and short (130 nm, blue traces) SEC fractions from starting materials of different purity: (A) CoMoCAT SWCNTs without prepurification, (B) CoMoCAT SWCNTs prepurified by ultracentrifugation, (C) semiconductor-enriched arc-discharge SWCNTs (IsoNanotube-S), and (D) empty-enriched arc-discharge SWCNTs. All spectra are normalized at the highest E_{22} transition peak.

the observed baseline levels? Further investigations are needed to fully address these questions. On the basis of our current data, we propose that the absorption baseline is largely due to the presence of defective tubes, which are effectively removed by the ultracentrifugation purification methods. Supporting this hypothesis is the resonance Raman measurement (see Figure S5 in the Supporting Information) we carried out on singly purified (SEC alone) and doubly purified (SEC + ultracentrifugation) CoMoCAT tubes of different lengths (Table 1). The G/D ratio, which is a measure of defect levels, is about the same for the long (360 nm) fractions but is different for the short fractions. It is 2-fold higher for the short fraction prepurified by ultracentrifugation.

We have also considered carbonaceous impurities as a potential source of the absorption baseline. In a previous study, we carefully examined carbonaceous impurities present in the CoMoCAT material and concluded that carbonaceous

Table 1. Quantification of Defect Density for Short (130 nm) and Long (360 nm) CoMoCAT SWCNT Fractions Singly Purified (by SEC) and Doubly Purified (By Ultracentrifugation Plus SEC)[a]

	long SWCNT fraction	short SWCNT fraction
singly purified:		
baseline absorbance	0.39	0.63
average curvature	0.5 ± 0.06 μm^{-1}	3.9 ± 0.5 μm^{-1}
G/D ratio	65 ± 4	32 ± 4
doubly purified:		
baseline absorbance	0.33	0.34
average curvature	0.6 ± 0.14 μm^{-1}	1.8 ± 0.4 μm^{-1}
G/D ratio	69 ± 4	64 ± 9

[a]Baseline absorbance is defined as in Figure 4. The ± sign indicates 95% confidence interval for the measurement.

impurities alone cannot account for the observed baseline level. On the other hand, we observed a large amount of curved tubes in short CoMoCAT fractions, suggesting that the baseline change is due to these curved defective SWCNTs that are more common among short tubes.[29] In Table 1, we provide further curvature quantification data showing that the SEC purified short CoMoCAT fraction has both a higher level of curved tubes and a higher level of defects as measured by the G/D ratio; upon ultracentrifugation both the curvature and defect level are reduced. In the case of arc and HiPco SWCNTs, we did not observe many curved nanotubes in AFM images of singly- or doubly-purified samples. Nevertheless, the decrease in length-dependent baseline change from 23% to 6% suggests that ultracentrifugation removes short defective arc tubes as well. It may be that for larger diameter tubes, defectiveness does not manifest as an increase in nanotube curvature.

Beyond the capability to produce length fractionated samples of consistent spectral characteristics, our findings have implications for the evaluation of SWCNT raw material quality. Most nanotube synthesis methods, including CoMoCAT,[25] HiPCO,[35] laser ablation,[33] and arc discharge,[27] produce nanotubes with baseline features which vary dramatically in length fractionated samples.[30] Our findings suggest that all of these materials contain substantial amounts of defective nanotubes, which concentrate in the short fractions. This may be due to slower growth rate of defective nanotubes or to the migration and accumulation of defects near a nanotube end during growth.[36] Regardless of their origins, the presence of defective nanotubes will impact those applications that use the raw nanotube material directly without purification or use length fractionated materials which do not have consistent absorption spectra. Our study shows that measuring the absorption spectra of length-fractionated SWCNT materials may be a convenient new way to evaluate their defect levels.

CONCLUSIONS

We have demonstrated the high-resolution length fractionation of surfactant dispersed SWCNTs by SEC. This method should be applicable to a wide range of nanotube materials dispersed with bile salts, including SWCNTs prepurified by other methods. The latter may include diameter sorted, empty-filled sorted, chirality sorted, or metal-semiconductor sorted samples. Furthermore, we have shown that samples produced by such double purification do not show variability in their optical spectra with length. To our knowledge, this is the first easily accessible method for producing high-resolution length sorted

dx.doi.org/10.1021/ac303349q | Anal. Chem. 2013, 85, 1382−1388

samples with invariant optical properties and the first bulk-sample demonstration of the principle that the optical properties of defect-free SWCNTs are length-independent. Finally, this method suggests a new way for evaluating defect levels in as-synthesized SWCNT materials, according to the optical absorption baseline change in length fractionated samples.

■ ASSOCIATED CONTENT

Supporting Information

Elution profiles of several runs, AFM images of long and short fractions of the double-purified CoMoCAT and empty/water-filled sorted arc-discharge materials, curvature quantification data for the CoMoCAT materials, and sample Raman spectra. This material is available free of charge via the Internet at http://pubs.acs.org.

■ AUTHOR INFORMATION

Corresponding Author

*E-mail: ming.zheng@nist.gov.

Notes

The authors declare no competing financial interest.

■ REFERENCES

(1) Liu, Z.; Tabakman, S.; Welsher, K.; Dai, H. *Nano Res.* **2009**, *2*, 85−120.
(2) Cherukuri, T. K.; Tsyboulski, D. A.; Weisman, R. B. *ACS Nano* **2012**, *6*, 843−850.
(3) Welsher, K.; Sherlock, S. P.; Dai, H. *Proc. Natl. Acad. Sci. U.S.A.* **2011**, *108*, 8943.
(4) Becker, M. L.; Fagan, J. A.; Gallant, N. D.; Bauer, B. J.; Bajpai, V.; Hobbie, E. K.; Lacerda, S. H.; Migler, K. B.; Jakupciak, J. P. *Adv. Mater.* **2007**, *19*, 939−945.
(5) Khripin, C. Y.; Arnold-Medabalimi, N.; Zheng, M. *ACS Nano* **2011**, *5*, 8258−8266.
(6) Zhang, L.; Tu, X.; Welsher, K.; Wang, X.; Zheng, M.; Dai, H. *J. Am. Chem. Soc.* **2009**, *131*, 2454−2455.
(7) Cleuziou, J. P.; Wernsdorfer, W.; Bouchiat, V.; Ondarçuhu, T.; Monthioux, M. *Nat. Nanotechnol.* **2006**, *1*, 53−59.
(8) Asada, Y.; Miyata, Y.; Shiozawa, K.; Ohno, Y.; Kitaura, R.; Mizutani, T.; Shinohara, H. *J. Phys. Chem.* **2010**, *115*, 270−273.
(9) Miyata, Y.; Shiozawa, K.; Asada, Y.; Ohno, Y.; Kitaura, R.; Mizutani, T.; Shinohara, H. *Nano Res.* **2011**, *4*, 963−970.
(10) Si, R.; Wang, H.; Wei, L.; Chen, Y.; Wang, Z.; Wei, J. *J. Mater. Res.* **2012**, *1*, 1−8.
(11) Duesberg, G. S.; Burghard, M.; Muster, J.; Philipp, G. *Chem. Commun.* **1998**, 435−436.
(12) Duesberg, G. S.; Muster, J.; Krstic, V.; Burghard, M.; Roth, S. *Appl. Phys. A: Mater. Sci. Process.* **1998**, *67*, 117−119.
(13) Huang, X.; Mclean, R. S.; Zheng, M. *Anal. Chem.* **2005**, *77*, 6225−6228.
(14) Chen, B.; Selegue, J. *Anal. Chem.* **2002**, *74*, 4774−4780.
(15) Chun, J.; Fagan, J. A.; Hobbie, E. K.; Bauer, B. J. *Anal. Chem.* **2008**, *80*, 2514−2523.
(16) Heller, D. A.; Mayrhofer, R. M.; Baik, S.; Grinkova, Y. V.; Usrey, M. L.; Strano, M. S. *J. Am. Chem. Soc.* **2004**, *126*, 14567−14573.
(17) Sun, X.; Zaric, S.; Daranciang, D.; Welsher, K.; Lu, Y.; Li, X.; Dai, H. *J. Am. Chem. Soc.* **2008**, *130*, 6551−6555.
(18) Fagan, J. A.; Becker, M. L.; Chun, J.; Hobbie, E. K. *Adv. Mater.* **2008**, *20*, 1609−1613.
(19) Ohmori, S.; Saito, T.; Shukla, B.; Yumura, M.; Iijima, S. *ACS Nano* **2010**, *4*, 3606−3610.
(20) Khripin, C. Y.; Manohar, S.; Zheng, M.; Jagota, A. *J. Phys. Chem. C* **2009**, *113*, 13616−13621.
(21) Hennrich, F.; Krupke, R.; Arnold, K.; Rojas Stütz, J. A.; Lebedkin, S.; Koch, T.; Schimmel, T.; Kappes, M. M. *J. Phys. Chem. B* **2007**, *111*, 1932−1937.
(22) Hersam, M. *Nat. Nanotechnol.* **2008**, *3*, 387−394.
(23) Liu, J.; Hersam, M. C. *MRS Bull.* **2010**, *35*, 315−322.
(24) Liu, H.; Nishide, D.; Tanaka, T.; Kataura, H. *Nat. Commun.* **2011**, *2*, 309.
(25) Haggenmueller, R.; Rahatekar, S. S.; Fagan, J. A.; Chun, J.; Becker, M. L.; Naik, R. R.; Krauss, T.; Carlson, L.; Kadla, J. F.; Trulove, P. C.; Fox, D. F.; DeLong, H. C.; Fang, Z.; Kelley, S. O.; Gilman, J. W. *Langmuir* **2008**, *24*, 5070−5078.
(26) Certain commercial equipment, instruments, or materials are identified in this paper in order to specify the experimental procedure adequately. Such identification is not intended to imply recommendation or endorsement by the National Institute of Standards and Technology nor is it intended to imply that the materials or equipment identified are necessarily the best available for the purpose. Unless noted otherwise, all reagents were obtained from standard sources.
(27) Fagan, J. A.; Huh, J. Y.; Simpson, J. R.; Blackburn, J. L.; Holt, J. M.; Larsen, B. A.; Hight Walker, A. R. *ACS Nano* **2011**, *5*, 3943−3953.
(28) Giddings, J. C.; Kucera, E.; Russell, C. P.; Myers, M. N. *J. Phys. Chem.* **1968**, *72*, 4397−4408.
(29) Khripin, C. Y.; Tu, X.; Howarter, J. A.; Fagan, J. A.; Zheng, M. *Anal. Chem.* **2012**, *84*, 8733−8739.
(30) Fagan, J. A.; Simpson, J. R.; Bauer, B. J.; Lacerda, S. H. D. P.; Becker, M. L.; Chun, J.; Migler, K. B.; Walker, A. R. H.; Hobbie, E. K. *J. Am. Chem. Soc.* **2007**, *129*, 10607−10612.
(31) Tu, X.; Hight-Walker, A. R.; Khripin, C. Y.; Zheng, M. *J. Am. Chem. Soc.* **2011**, *133*, 12998−13001.
(32) Skoog, D. A.; West, D. M. *Principles of Instrumental Analysis*, 5th ed.; Saunders College: Philadelphia, PA, 1998.
(33) Arnold, M. S.; Green, A. A.; Hulvat, J. F.; Stupp, S. I.; Hersam, M. C. *Nat. Nanotechnol.* **2006**, *1*, 60−65.
(34) Naumov, A. V.; Ghosh, S.; Tsyboulski, D. A.; Bachilo, S. M.; Weisman, R. B. *ACS Nano* **2011**, *5*, 1639−1648.
(35) Tu, X.; Manohar, S.; Jagota, A.; Zheng, M. *Nature* **2009**, *460*, 250−253.
(36) Lu, J.; Miao, J. *Nanoscale Res. Lett.* **2012**, *7*, 356.